Measurements on top quark pairs in proton collisions recorded with the ATLAS detector

Mussche, I.

Publication date
2012

5 Measurement of the $t\bar{t}$ production cross section

This chapter describes the measurement of the production cross section of top quark pairs ($t\bar{t}$), performed with the full data set recorded by the ATLAS detector in 2010. The production rate of top quark pairs is measured by the CDF [78] and D0 [79] collaborations for a CM-energy of 1.96 TeV, at the Tevatron. ATLAS presented a measurement that confirmed top quark pair production in the proton-proton collisions with a CM-energy of 7 TeV at the LHC, with the first 3 pb^{-1} of data [80]. The measurement in this chapter (using 35 pb^{-1}) aims to establish the cross section in the single-lepton decay channel of $t\bar{t}$ events.

The analysis that is conducted is based on a 'simultaneous template fit'. The preselected data are categorized in subsets, characterized by having different jet multiplicities and a different number of b-tagged jets. The expected signal-to-background ratio differs between each subset. We established template shapes of the invariant mass distribution of the top quark for the expected signal and background, in each of these subsets. Data-driven constraints relate the number of signal and background events in the different subsets. The templates are then fitted to the data in the six subsets of the data simultaneously, respecting the constraints. The estimate of the total number of signal events in the complete data set that follows from this procedure is directly proportional to the top quark production cross section.

The chapter is outlined as follows. We first introduce the fit method and likelihood construction. The sections that follow describe the input components to the fit, the subdivision of the data and the expected component of signal and background in the resulting subsets. Thereafter, the fit ratio measurements and template extraction are discussed. Finally, we present the results and estimates of the systematic uncertainties

that are introduced throughout the procedure.

5.1 The simultaneous template fit

The measurement of the top quark production cross section with b-tagging is done by fitting shape templates to the invariant mass distribution of the hadronic top, m_{jjj}. We use the KL-fitter reconstruction algorithm or the $\sum_{p_T}$ algorithm (Section 4.7) to obtain m_{jjj}, depending on the number of jets in the event. The concept behind this measurement is to slice the data into six subsamples with different compositions of $t\bar{t}$ and background events. We categorize each event by its jet multiplicity and b-jet multiplicity: the number of jets can be either 3, or ≥ 4 (events with less jets were omitted before), the number of b-jets can take values of 0, 1, or ≥ 2.

In the events with low jet multiplicity and without b-tags high background is expected, as a decaying $t\bar{t}$ pair should produce at least four jets, with a high probability of at least one b-tag. In the slices of data with 4 or more jets, of which some are b-tagged, relatively more signal will be present. The reason for including the 3-jet events into the analysis is that it improves the background characterization in the 4-jet slice.

The power of the simultaneous fit comes from the constraints that relate the six subsets. It is possible to define ratios that predict the population of one slice by extrapolation from another slice of data. The values and uncertainties of three of such ratios are measured externally and are included to the likelihood to constrain the fit and improve the result. Two constraints are implemented as Gaussian PDFs that have a mean and width estimated from data-driven methods. They are allowed to vary within this range, according to the Gaussian shape. The third ratio is fixed to the value obtained from simulation. The following sections cover the details on the estimation of these constrained ratios. Besides the data-driven constraint estimates, the shape templates for the background are taken from data control samples as well. The implementation of data-driven methods reduces the overall dependency on Monte Carlo simulations, with the aim to suppress systematic uncertainties.

5.1.1 The construction of the fit

We use twelve templates to fit to the invariant mass (m_{jjj}) distributions in six subregions (slices) of phase space. The contributions to the likelihood for each slice of data can be expressed as

$$[f(x)]_i^j = [N_B \cdot \mathcal{T}_B(x) + N_S \cdot \mathcal{T}_S(x)]_i^j,$$

where $x = m_{jjj}$ and i, j being the number of jets and b-tags respectively. The signal and background templates $\mathcal{T}_S$ and $\mathcal{T}_B$ are separately defined for each subsample. Hence we have twelve normalized templates as a fixed input to the fit. The template construction is described in Section 5.4. The function $f(x)$ is the measured spectrum in the category corresponding to indices i and j. N_B and N_S are scalar fit parameters.

Figure 5.1 shows a schematic view of the subsamples. The six boxes on the left represent the six subsamples, each built up out of a signal and background contribution, $[N_S]_i^j$ and $[N_B]_i^j$. The sum of all events with 3 jets and all events with $\geq$4 jets is shown on the right. In the following our notation will be $[N_S]_4 = \sum_{j=0}^{2}([N_S]_4^j)$, and $[N_S]_3 = \sum_{j=0}^{2}([N_S]_3^j)$, i.e., summing over all b-tag slices.

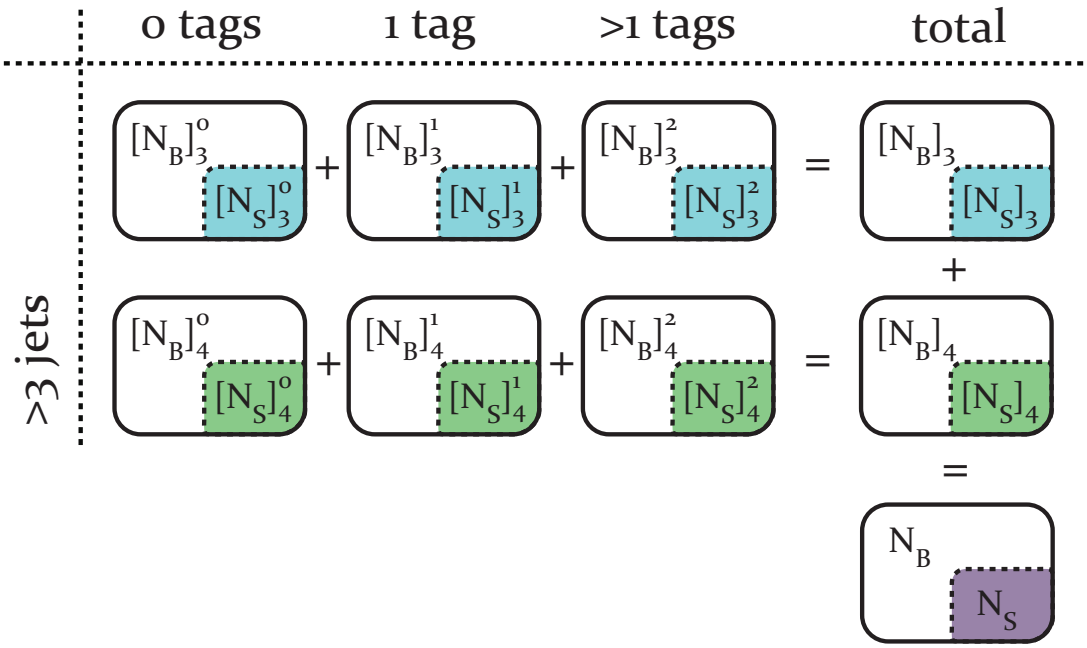

Figure 5.1 – Overview of the structure of subsamples. The white region of the square represents the background and the colored region indicates the signal. The six squares on the left side correspond to the data slices. The horizontal and vertical sum are used as well.

The six data slices are fitted simultaneously to make use of several connections amongst them. We define three ratios:

$$
\begin{aligned}
R_1 &= [N_B]_3^1/[N_B]_3 && \text{(constrained)},\\
R_2 &= [N_S]_4/[N_S]_3 && \text{(constrained)},\\
R_3 &= \frac{[N_B]_3^1/[N_B]_3}{[N_B]_4^1/[N_B]_4}. && \text{(fixed)}
\end{aligned}
$$

The ratios, relating the subsets in the fit in different ways (see Figure 5.1), are measured externally, as supplemental input to the likelihood. The subsidiary measurements are implemented as a Gaussian distribution for the ratios R_1 and R_2, for R_3 we obtain a value direct from simulation. Section 5.3 treats the measurement of these ratios and discusses the reasons that motivate the choice of the ratios. We define the likelihood in

five terms:

$$\mathcal{L} = \prod_{n=1}^{N_{evts}} \underbrace{\left(\prod_{i=3}^{4}\prod_{j=0}^{2} \frac{[f(x)]_i^j}{[N_S]_i^j + [N_B]_i^j}\right)}_{\text{Template PDFs}} \cdot \underbrace{P(N_{obs}; N_S, N_B)}_{\text{Poissonian}} \cdot \underbrace{G_1(\tilde{R_1}; R_1, \sigma_1)}_{\text{Gaussian}} \cdot \underbrace{G_2(\tilde{R_2}; R_2, \sigma_2)}_{\text{Gaussian}} \cdot \underbrace{\delta(\tilde{R_3}; R_3)}_{\text{Delta}}. \quad (5.1)$$

In the first term, the six fit equations $[f(x)]_i^j$ describing the template probability density functions are normalized by the total number of events in that slice. This term is the core of the simultaneous template fit. The Poissonian term is introduced to treat the total number of events as a random variable, rather than a fixed number. This allows the total number of events to be adjusted during minimization (of the negative log of the likelihood, $-log(\mathcal{L})$), if the fit requires it. Then there are two Gaussian terms for the ratios $\tilde{R_1}$ and $\tilde{R_2}$, with a mean R and width σ obtained from subsidiary measurements. Finally, there is a delta function, representing the inclusion of a fixed ratio R_3, also obtained externally. Section 5.3 is dedicated to the determination of the central value and of the ranges the first two fractions are allowed to vary within. The negative log of this likelihood is minimized with MINUIT [81].

The six output parameters can be reparametrized in several ways. The total number of signal events is the measure for the cross section calculation. As a spin-off, we can extract the efficiency of tagging a b-quark from the fit result.

B-tagging efficiency

The efficiency for tagging a jet in $t\bar{t}$ events is derived from events with exactly three jets. We write the number of events in the 3-jet/1-tag subset as a function of the true jet originators, i.e., b-quarks, light quarks or tau leptons. To do so, we define f_{qqq}, f_{qqb} and f_{qbb} where the subscript indicates how many of the jets came from b-quarks. From signal simulation it follows that the fraction of events with exactly three jets, where the jets originate from two b-quarks and one other object (usually quarks), f_{qbb} is 64.7%. Similarly, f_{qqb} is 32.0% and f_{qqq} is 3.5%, all obtained from simulation [1]. The probability of each of these topologies to end up in the 3-jet/1-tag category depends directly on the b-tag efficiency and the fake rate. The fake rate r_f is defined as the fraction of non-b particles or partons that get misidentified b-quark jets. We define the efficiency $[\epsilon_S]_3^1$ as

[1] The difference between the percentages of f_{qqb} and f_{qbb} comes from kinematical arguments. At least one jet is not detected in 3-jet events that come from $t\bar{t}$. The b-jet is on average produced with a higher momentum than the other decay products and is more often detected.

the ratio of events with one b-tag, normalized to all events with three jets as:

$$[\epsilon_S]_3^1 = \frac{[N_S]_3^1}{[N_S]_3} = f_{qbb} \cdot (2 \cdot (1 - r_f) \cdot B_{\mathit{eff}} \cdot (1 - B_{\mathit{eff}}) + (1 - B_{\mathit{eff}})^2 \cdot r_f) + f_{qqb} \cdot ((1 - r_f)^2 \cdot B_{\mathit{eff}} + 2 \cdot r_f \cdot (1 - r_f) \cdot (1 - B_{\mathit{eff}})) + f_{qqq} \cdot 3 \cdot r_f \cdot (1 - r_f)^2,$$

with $[\epsilon_S]_3^1$ a parameter that is determined by the fit. The b-tag efficiency (B_{eff}) and fake rate (r_f) are unknowns and need to be determined from the data. Under the assumption that the fake rate is small (in simulation we find a value of 0.025 for r_f), the expression above simplifies to

$$[\epsilon_S]_3^1 = f_{qbb} \cdot 2 \cdot B_{\mathit{eff}} \cdot (1 - B_{\mathit{eff}}) + f_{qqb} \cdot B_{\mathit{eff}}.$$

As we neglect the fake rate, the b-tag efficiency can be extracted from this equation. Systematic uncertainties are assigned to the values of f_{qbb} and f_{qqb}, since they are obtained from simulation. Likewise an uncertainty is considered for the fake rate approximation. The additional results obtained from this aspect of the fit are discussed in Section 5.5.

5.2 Properties of data

The input to the fit procedure consists of several elements: template shapes of the signal and background, constraints on ratio parameters, and finally the data distributions of m_{jjj} in each subset.

5.2.1 Data categorization

The data set that is used in this analysis is described in the previous chapter, as well as the selection requirements and reconstruction. In this section we create the six subsets of data that are used in the fit, as described earlier. The normalization of the categories for the electron channel is shown in Table 5.1 for the signal ($t\bar{t}$), sum of all background events, and data. The sum of all backgrounds contains $W+$jets, $Z+$jets, diboson, single top and multijet events. The uncertainty reflects the statistical uncertainty, except for the data-driven multijet component in background events, to which a systematic uncertainty is added. In the electron channel the data is compatible with expected values, within uncertainties. This is true for the ensemble, some of the subsets show discrepancies larger than 1σ.

A more schematic view of the relative population per bin in the electron channel is shown in Figure 5.2(a). Each of the six squares shows the amount of signal and background in a specific subregion, together with the data values. The signal and background are depicted with histograms in light and dark gray. The data are shown with the black

Table 5.1 – Expected and observed event yields in electron channel. The error margins reflect the statistical uncertainty, except for the multijet background where the systematic uncertainty is added.

	$t\bar{t}$	Sum of bkgs	S/B	Total Exp.	Data
3-jet exclusive					
0 *b*-tag	38.5 ± 0.4	606.7 ± 32.9	0.1	645.2 ± 32.9	593 ± 24
1 *b*-tag	56.3 ± 0.5	46.3 ± 7.4	1.2	102.6 ± 7.4	134 ± 12
>1 *b*-tags	20.6 ± 0.3	5.7 ± 2.2	3.6	26.4 ± 2.2	39 ± 6
Total	115.4 ± 0.8	658.8 ± 42.3	0.2	774.2 ± 42.3	766 ± 28
4-jet inclusive					
0 *b*-tag	51.7 ± 0.5	196.1 ± 13.3	0.3	247.8 ± 13.4	239 ± 15
1 *b*-tag	91.9 ± 0.7	25.9 ± 6.1	3.5	117.8 ± 6.1	110 ± 10
>1 *b*-tags	45.9 ± 0.5	6.4 ± 2.7	7.2	52.3 ± 2.7	48 ± 7
Total	189.5 ± 1.0	228.4 ± 22.0	0.8	417.9 ± 22.0	397 ± 20

Table 5.2 – Expected and observed event yields in muon channel. The error margins reflect the statistical uncertainty, except for the multijet background where the systematic uncertainty is added.

	$t\bar{t}$	Sum of bkgs	S/B	Total Exp.	Data
3-jet exclusive					
0 *b*-tag	55.4 ± 0.5	1116.0 ± 28.9	0.0	1171.4 ± 28.9	1116 ± 33
1 *b*-tag	79.1 ± 0.6	79.3 ± 9.8	1.0	158.4 ± 9.8	183 ± 14
>1 *b*-tags	29.1 ± 0.4	6.2 ± 0.3	4.7	35.3 ± 0.5	39 ± 6
Total	163.6 ± 0.9	1269.8 ± 106.7	0.1	1433.4 ± 106.7	1338 ± 37
4-jet inclusive					
0 *b*-tag	73.5 ± 0.6	320.6 ± 8.6	0.2	394.1 ± 8.6	401 ± 20
1 *b*-tag	133.6 ± 0.8	42.8 ± 9.0	3.1	176.4 ± 9.0	169 ± 13
>1 *b*-tags	67.4 ± 0.6	5.4 ± 0.4	12.4	72.9 ± 0.7	76 ± 9
Total	274.5 ± 1.2	403.1 ± 51.5	0.7	677.6 ± 51.5	646 ± 25

circles. In the bins with b-tagged jets, the absolute normalization (scale) is adjusted ($\times 4$ and $\times 10$) for both the signal and background component, for visibility reasons. The aim is to emphasize the signal to background (S/B) ratio rather than the absolute differences in numbers of events. The maximal value of S/B is 7.3 in the subset with four or more jets of which at least two are b-tagged. The discrepancies between the central values of data and expectation emerge especially in the 3-jet subsets, where the number of b-tagged jets is underestimated. The difference is covered by the statistical uncertainties on the values, however.

For the muon channel the signal and background estimates in the different bins are displayed in Table 5.2 and Figure 5.2(b). The number of events in the muon channel is about twice as high as the electron channel, making it less vulnerable to statistical fluctuations. The agreement between data and simulation is good, even better than in the electron channel. The S/B ratio varies from 0.1 (3-jet/0-tag) to 12.5 (in the 4-jet/>1-tags subset), which proves the goal of the categorization is reached in simulation at least.

5.3 Extraction of ratios

As mentioned before, we include three subsidiary measurements on ratios in the likelihood of the fit. Two are introduced as a Gaussian probability density function, with a predefined mean and resolution.

The Gaussian constraints on the relation between the six subsets in the constructed likelihood reduce the statistical uncertainty on the measured cross section. It is possible to define numerous ratios that fix or constrain the relation between the background in two different subsets, but the constraints on the relation can rely only partly on data-driven methods. Therefore it is not advantageous to insert too many constraints as this will increase the systematic uncertainty as a result of the simulation dependence. The best results in terms of the reduction of the total uncertainty are obtained by adding one fixed ratio as well (R_3), which is discussed in Section 5.3.3.

5.3.1 First fit ratio and heavy flavor uncertainty

The approach that is chosen for the extraction of the first fit ratio (R_1) limits the range of the tagging rate in background events by extrapolating from information in the 2-jet data sample. The 2-jet events form a control region orthogonal to the data used in our measurement and contain a large fraction of background events. We can define an extrapolation factor $f^{\hat{j}}_{2\to 3}$. It relates the 2-jet efficiency that can be obtained from data to the 3-jet efficiency that will be constrained:

$$[\epsilon_B]^{\hat{j}}_3 = f^{\hat{j}}_{2\to 3} \cdot [\epsilon_B]^{\hat{j}}_2, \tag{5.1}$$

where $[\epsilon_B]^{\hat{j}}_2$ is the background tagging efficiency in 2-jet events, for a certain b-tag requirement $\hat{j}$. And $[\epsilon_B]^{\hat{j}}_2$ is the equivalent variable in 3-jet events. The index $\hat{j}$ is extended

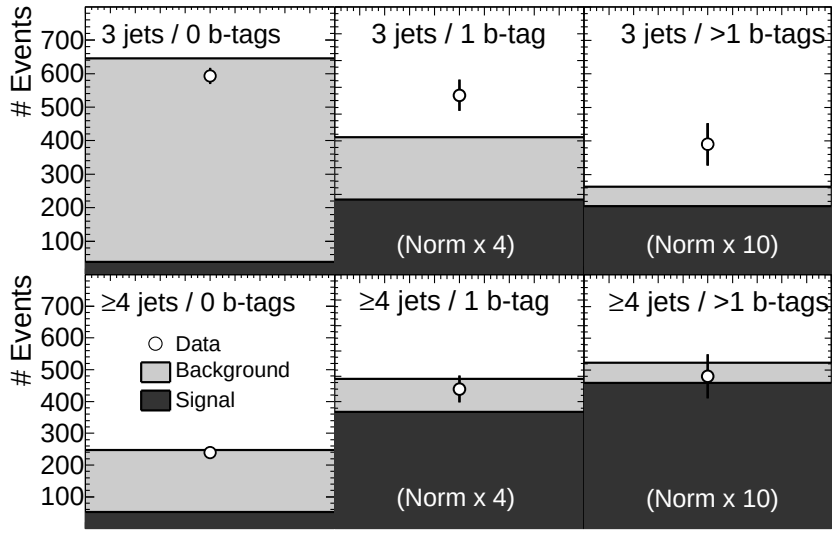

(a)

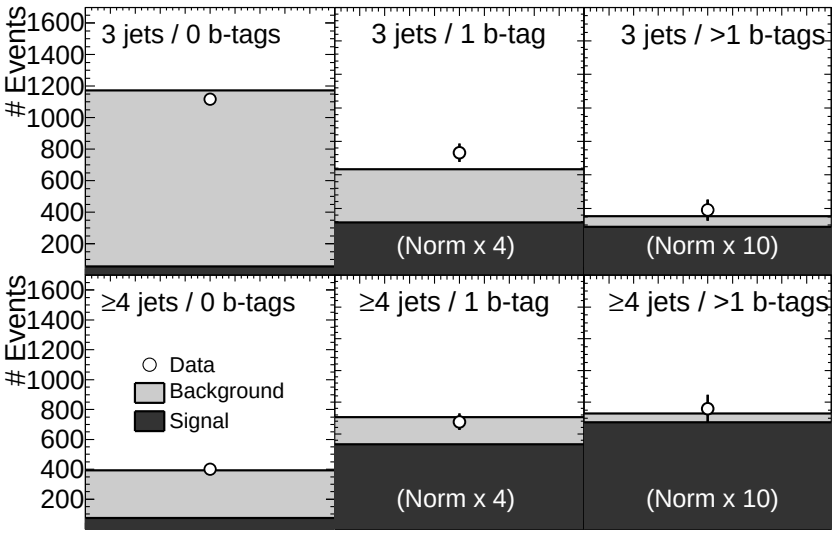

(b)

Figure 5.2 – Bin population in the electron channel (a) and muon channel (b). The bins with b-tagged events in both signal and background are scaled up with a factor 4 or 10 to match the labeling of the y-axis. No relative scaling between signal and background is applied.

from the index j we used so far. It can assume three values: (1) one b-tag inclusive, (2) one b-tag exclusive, (3) two b-tags inclusive. Note that a zero b-tag exclusive value is 100% anti-correlated with (1). We will determine which configuration to use, based on which gives the smallest overall uncertainties. The result is shown later in this section. Simulation gives an estimate of the factor $f^{\hat{j}}_{2\to 3}$, but we obtain the value of the variable

$[\epsilon_B]_2^1$ from data. We measure the number of events of data after all selection with exactly two jets and subtract the number of expected signal events from it:

$$[\epsilon_B]_2^{\hat{j}} = \frac{N_2^{\hat{j}} \text{ (data)} - [N_S]_2^{\hat{j}} \text{ (sim.)}}{N_2 \text{ (data)} - [N_S]_2 \text{ (sim.)}} \tag{5.2}$$

$N_2^{\hat{j}}$ is total number of events with two jets in data, $[N_S]_2^{\hat{j}}$ is the amount of $t\bar{t}$ events in this slice, established from simulated events. Background events dominate this control region. N_2 and $[N_S]_2$ are numbers of events without any b-tag requirement. To the number of $t\bar{t}$ events in the 2-jet bin that is obtained from simulation, we assign a 100% uncertainty, because this contains the signal process that we are trying to measure.

In conclusion, there are three configurations for $f_{2\to3}$ to choose from, which we test with respect to the impact the heavy flavor uncertainty on $W+$jets in the following.

Uncertainty of heavy flavors in $W+$jets.

One important aspect in the background estimates is the presence of b- and c-quarks (heavy quark flavors) in the production of $W+$jets. The quark flavor composition of the $W+$jets background is not well known; there is a large uncertainty on the number of c- or b-quarks in this background[2]. An under- or overestimate of the number of c- or b-quarks in the $W+$jets background can severely affect our measurement of the cross section. The dependency of the likelihood on this uncertainty is introduced when we apply b-tagging: the subset populations migrate when the composition of b- and c-quarks is modified. And hence the connections between the amount of background in the subsets and therefore the fit constraints change. This is unavoidable to some extent, but we attempt to minimize the sensitivity to this specific uncertainty.

Treatment of heavy flavors in $W+$jets simulation

The simulation of the hard process or matrix element of $W+$jets production in this analysis is performed with ALPGEN. But, the hadronization and parton shower are done in HERWIG. Matching is applied to assign jets produced in the shower to partons of the matrix element. That means that if a jet does not match with one of the partons of the matrix element, that event is vetoed. In this way it is possible to define samples with a fixed number of partons with certain kinematic properties.

In the primary sample, events with N number of partons are produced ($W + Np$), where the partons are treated as massless. We refer to the the primary sample as '$W+$light jets'. Next to $W+$light jets ALPGEN separately produces $W+c$, $W+c\bar{c}$, and $W+b\bar{b}$ samples. In this case the c- and b-quarks are treated as partons with mass. ($W+c$ includes $W+\bar{c}$.)

[2]The same is true for $Z+$jets. We do not discuss heavy flavor uncertainty in $Z+$jets, because this background is negligible in the decay channel of subject.

The use of the ensemble of the above described W boson production suffers from overlap between samples. For example an event with a $b\bar{b}$ pair can be generated in '$W+2$light jets' and in $W+b\bar{b}$. To solve this, first of all events are vetoed from the W+light jets sample when any c- or b-quarks are present in the matrix element. Secondly, events are classified according to the opening angle between two heavy quarks, if present. This choice is based on the knowledge that the matrix element is best suited for large opening angles and the parton shower on the other hand describes collinear quarks better. A threshold of 0.4 for the opening angle ΔR is set: above this value the matrix element is favored and below this value the parton shower description.

That means that events in W+light jets and $W+c$ are removed if a heavy quark pair with $\Delta R > 0.4$ is produced in the parton shower. In $W+c\bar{c}$ events are vetoed if ΔR of the created $c\bar{c}$ pair in the matrix element is below 0.4, or if a $b\bar{b}$ pair with opening angle above 0.4 is found in the parton shower. Similarly in $W+b\bar{b}$ events are omitted if the $b\bar{b}$ pair in the matrix element has an opening angle below threshold.

This leaves us with a orthogonal and complete set of simulated $W+$jets events. Depending on the number of extra jets in the subsample, the fraction of removed events ranges from 5 to 10%. We use the classification and its uncertainty as tools for the calculation of uncertainty of the relative ratios of these events.

Observations from $W+$jets in data

It is not possible to obtain a pure sample of $W+$jets events in data if more than three jets are involved, as it is not possible to isolate $W+$jets events from the $t\bar{t}$ contamination in this region. In 2-jet events it is easier, however. The fraction of b-tagged events among $W+2$ jets events is measured in data and shows an underestimation of the $W+b\bar{b}$ and $W+c\bar{c}$ fractions of 30% [82]. Our estimates of these two fractions are corrected for this observation in the analysis and a 50% (correlated) uncertainty is assigned to this correction that is obtained from internal ALPGEN generator studies. Similarly, an uncertainty of 40% on the fraction of $W+c$ events without a shift of the central value is deduced [82].

Figure 5.3 shows the distribution of m_T^W in the 2-jet (left) and 3-jet (right) channel for the different contributions of $W+$jets (no other background included) in simulation. The 30% correction is applied to simulation in these distributions. The plots in the top represent events after all selection cuts except b-tagging. The contribution of light quarks in the ensemble is 76% (70%) in the 2-jet (3-jet) events. The heavy quark contribution of 25-30% stems from $W+c$ and $W+c\bar{c}$ mostly, for the remainder $W+b\bar{b}$ contributes. The bottom plots (c,d) contain events that have at least one b-tagged jet in the event. Here, the fraction of events coming from heavy flavors is about 80%, of which $W+b\bar{b}$ now contributes significantly, especially in the 3-jet events, 37% of the total number of events. If the uncertainty of the heavy flavor fraction, and the uncertainty within the different types of heavy flavors are considered, this figure proves that it is important that the uncertainty on the heavy flavor fractions are handled well.

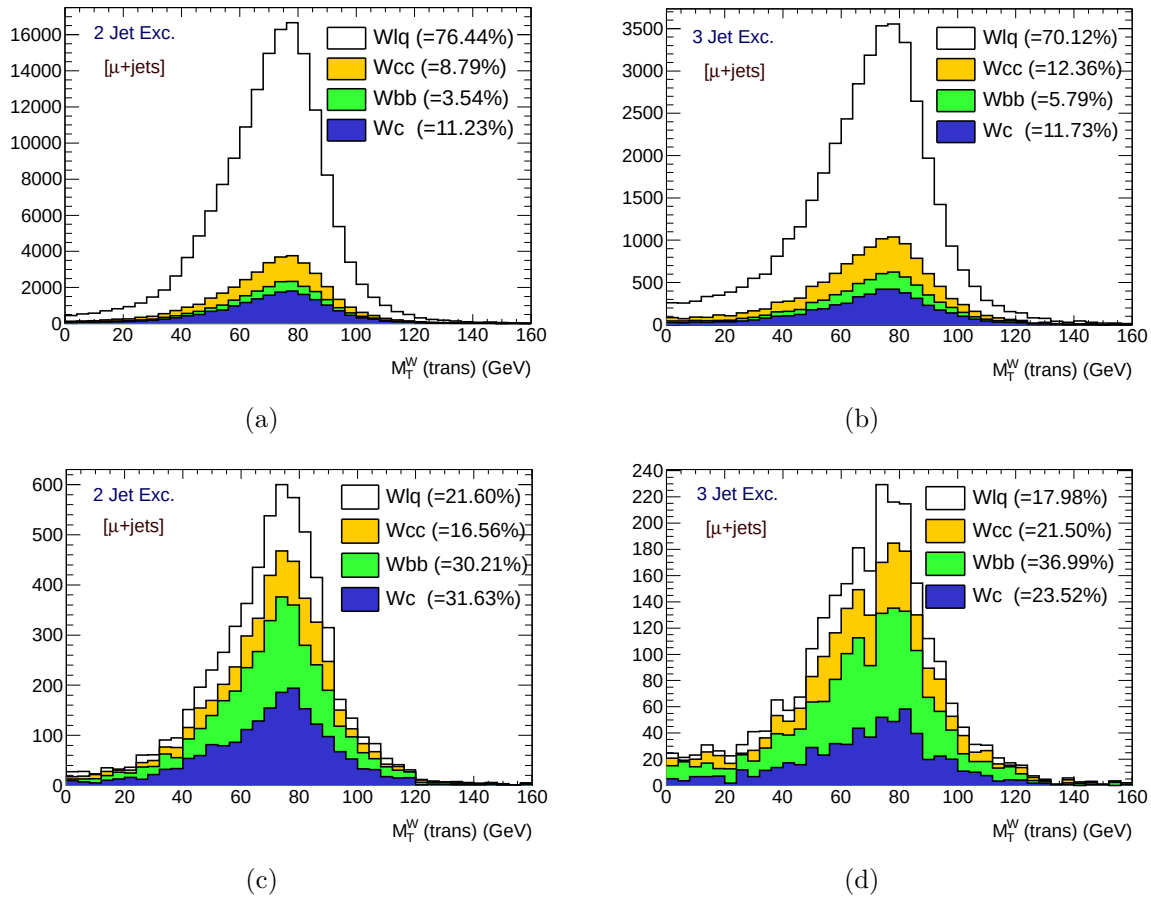

Figure 5.3 – Heavy flavor contributions in the $W+$jets background in simulation in the muon channel, in 2-jet and 3-jet events after all cuts, except b-tagging (a,b). The bottom plots show the equivalent plots after additionally requiring at least one b-tag.

Variations with respect to extrapolation factor

We use the uncertainties on the fraction of $W+c\bar{c}$ and $W+b\bar{b}$ events as described above. Events are reweighted following the maximally and minimally shifted values of the fraction of the respective types, simultaneously for $W+c\bar{c}$ and $W+b\bar{b}$ (similar production mechanisms), but separately for $W+c$. This results in 2x2 samples. Note that only the fraction is varied: in all cases the total number of events of $W+$jets is kept equal. Normalization uncertainties are assigned elsewhere.

Secondly, variations are applied in specific jet multiplicity slices of the data to account for possible correlated or uncorrelated behavior within the jet multiplicity. An additional 20% uncertainty in the 3-jet slice that is assumed to be uncorrelated is applied.

We return to the three alternatives for $f^{\hat{j}}_{2\to 3}$. As explained previously, they differ only in the number of b-tags that is included in the b-tag efficiency (1-tag exclusive and 1-tag or

2-tag inclusive)[3]. The different variations in heavy flavor fractions are applied separately. The quadratic sum of all deviations from the nominal value of the respective extrapolation factor is taken as indication for the final uncertainty on R_1.

The systematic uncertainty due to heavy flavor uncertainty (HF) on the scale factors are shown in Table 5.3 and are compared to the statistical uncertainty. The statistical uncertainty dominates, in each case. Although the uncertainty on the heavy flavor is of order 15%, we cannot make conclusive statements on the final uncertainty due to the limited number of events in simulation. Especially in the 2-tag bin, there are not enough events to establish a reasonable central value for $f^{\hat{j}}_{2\to 3}$ that can be used in the fit. The other two possibilities are comparable, in both their statistical and systematic uncertainty. This is true in both the e+jets and the μ+jets channel.

Concerning the uncertainty on $[\epsilon_B]^{\hat{j}}_2$, the 1-tag exclusive bin suffers less from the 100% uncertainty that is assigned to the $t\bar{t}$ subtraction step in Eq. 5.2.

In conclusion, we obtain the lowest total uncertainty, on the product $[\epsilon_B]_2 \cdot f_{2\to 3}$ for the 1-tag exclusive bin compared to the 1-tag exclusive bin: 40% vs. 44% for the electron channel and 26% vs. 28% in the muon channel.

Table 5.3 – Intermediate uncertainties on scale factors $f^{\hat{j}}_{2\to 3}$.

	$\mathbf{f^{\hat{j}}_{2\to 3}}$	**Stat. uncertainty**	**HF uncertainty**
e+jets	1-tag incl.	25.0 %	+15.6 / -15.8 %
	1-tag excl.	29.6 %	+16.2 / -16.4 %
	2-tag incl.	81.5 %	+11.3 / -11.2 %
μ+jets	1-tag incl.	19.3 %	+17.4 / -17.7 %
	1-tag excl.	22.5 %	+17.3 / -17.6 %
	2-tag incl.	57.3 %	+18.3 / -18.1 %

The nominal value of $[\epsilon_B]^1_3$ is 0.065 (0.085) for the electron (muon) channel to which we associate the uncertainty obtained by the procedure above. The central value and uncertainty define the mean and sigma in the Gaussian term in the fit, R_1 and σ_1.

5.3.2 Second fit ratio

The numbers of events per jet multiplicity for signal events are related through the ratio $R_2 = [N_S]_4/[N_S]_3$. This applies to the total sum of signal events per jet bin, independently of the population in terms of b-tag multiplicity. Although these ratios can be defined for

[3]More involved extrapolation factors were tested as well, taking into account more than one b-tag requirement, but in all cases systematic effects inflated.

both signal and background, only the one for signal is constrained in the fit by a Gaussian function, with a mean and width computed from simulation. The mean is acquired by performing the fit on the simulation of signal generated by MC@NLO. This central value is compared to the values coming from alternative signal simulation samples (POWHEG, ACERMC). The width is determined by the quadratic sum of the variation between the simulated samples of the different generators. For the electron channel the value is 1.57 ± 0.31, for the muons 1.60 ± 0.31. These numbers correspond to R_2 and σ_2 in the likelihood description (Eq. 5.1).

5.3.3 Third fit ratio

The third ratio is $R_3 = \frac{[N_B]_3^1/[N_B]_3}{[N_B]_4^1/[N_B]_4}$. The values are 1.65 in the electron channel, and 1.54 in the muon channel. They follow directly from simulated samples, although for the multijet contribution in background data is used. Test fits showed the best trade-off between statistical and systematical uncertainty when implementing the PDF as a delta function.

5.4 Construction of the templates

The shape templates of the m_{jjj} distribution in the several subsets are derived in different ways for signal and background. The signal templates are constructed from simulated distributions, whilst for the background shapes they are obtained from data.

5.4.1 Background templates

The background events passing our selection come from several sources, of which $W+$jets events contribute most. It is shown that the shape of m_{jjj} for all background sources can approximately be described by the same function, if all selection cuts are applied [83]. We exploit the fact that the associated jets in W boson production and multijets produce similar shapes for the mass of the three-jet combination. The shape is that of an exponential with a cut-off at low mass. Since $W+$jets events are difficult to isolate from $t\bar{t}$ events in data, we derive their shape from multijet background events, in data.

The number of events coming from multijet production passing our selection is limited. We therefore examine a complementary sample of data where the amount of multijet events is enhanced. This sample is defined by 'inverting' the lepton requirement: all events that contain a lepton satisfying the quality cuts are removed. All other cuts used for the nominal selection remain identical, except for the dedicated multijet-removing cut containing the transverse W boson mass. As we veto good leptons, the reconstruction of m_T^W is affected, because computing this observable requires a lepton candidate. But, events that pass our trigger selection must have a lepton candidate which, due to the inverted selection, by construction must be of lower quality. One source of these low quality leptons are fake leptons. This can be a jet that is misidentified as an electron, because deposits in the hadronic calorimeter were below threshold. Non-prompt leptons

are the other source. Those are leptons that do not originate from the hard process itself, but are produced somewhere in a secondary process (in a jet for example). Muons that pass the trigger and are not of good quality are mostly non-prompt, whereas electrons are mainly fakes. The reconstructed p_T threshold for these fake or non-prompt leptons is lowered from 20 GeV to 5 GeV. For each event that contains such a lepton that can be matched to a trigger hit, it is possible to reconstruct a value for m_T^W.

The obtained multijet enhanced sample is used to extract a fixed shape template for the distribution of m_{jjj} for the ensemble of $W+$jets, multijet and other background contributions. The fit requires six templates for the background, that is one template per subregion for all backgrounds. In the three-jet events, the KL-fitter reconstruction algorithm cannot be applied, as it requires at least four jets to work out the kinematics of the event. Therefore, for three-jet events we use the more straightforward $\sum p_T$ algorithm to reconstruct the mass of the hadronically decaying top, resulting in a wider peak around the top quark mass as we showed in Section 4.7.

The templates are obtained by fitting a hybrid smooth function to the respective samples. The function is composed of a Gaussian in the low mass region and an exponential on the high mass side:

$$f(x) = \begin{cases} \alpha e^{\frac{-(x-x_0)^2}{2\sigma^2}} & \text{for } x < x_c \\ \beta e^{\frac{-(x-x_0)}{2\gamma}} & \text{for } x \geq x_c \end{cases} \tag{5.3}$$

The cross over point between the two terms is $x_c = x_0 + \frac{1}{2}\sigma^2/\gamma$. This ensures the continuity and smoothness of the function. The function $f(x)$ is fitted to the distribution in each separate subset of data and physics channel. Figure 5.4 displays the curve resulting from the fit for one of the six bins: the data sample in the electron channel for the 3-jet/1-tag slice with inverted lepton cuts is fitted with the function $f(x)$. The fit in this example has a χ^2 per degree of freedom of 1.5.

5.4.2 Signal templates

In contrast to background, where we use data, we determined the different signal templates from simulation. This is done in each slice of number of jets and b-tags. The m_{jjj} distribution is built up from well-reconstructed top quarks and combinatorial background: from simulation we know that we in reality fail to correctly reconstruct all of the hadronic top quarks in the signal events. This is due to undetected objects (jets) or the wrong jet assignment in the algorithm. Also in case of signal we use the KL-Fitter for reconstruction of the top quarks in events with four or more jets and the $\sum p_T$ method for the 3-jet bins.

The analytic function we use to fit to the distribution is the same as for the background, but is extended by adding a Gaussian function, to parametrize the extra events in the top quark mass peak. The mean of the additional Gaussian is free to float in a window around 170 GeV. The fit results are displayed in Figure 5.5.

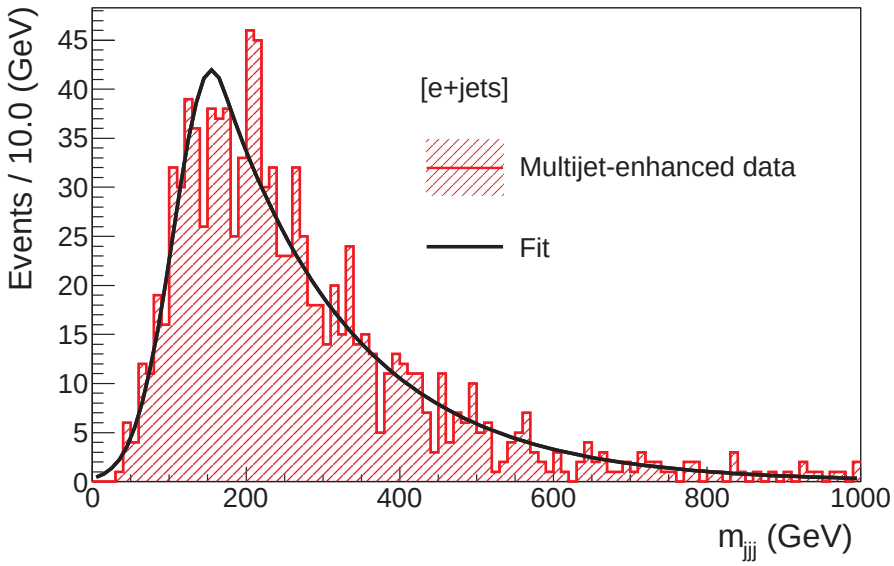

Figure 5.4 – Example of background template extraction in the 3-jet/1-tag subregion. The function in Eq. 5.3 is fitted to the m_{jjj} distribution (obtained with the $\sum p_T$ algorithm) in the multijet-enhanced data (dashed area) in the electron channel.

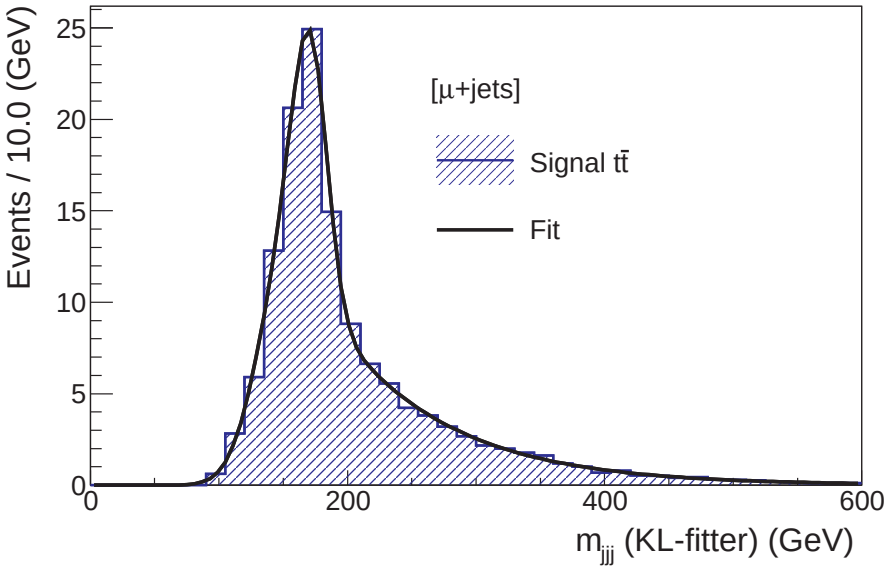

Figure 5.5 – Example of signal template extraction in the 4-jet/1-tag subregion. The distribution of the hadronic top mass as constructed with the KL-fitter in simulation of $t\bar{t}$ (dashed area) is fitted with the function in Eq. 5.3 with an additional Gaussian in the top pole mass region.

5.5 Fit results

The fit is applied to the electron and muon data separately. The resulting fit curves are shown in Figure 5.6. The figure shows the fit curves (solid line) for the six slices of data,

for both the electron (a) and the muon channel (b). The dashed line indicates the total background contribution.

Table 5.4 shows a summary of the fit results in terms of the relevant parameters: N_S, N_B and B_{eff}. The uncertainties reflect the statistical component only, evaluated with pseudo-experiments.

Table 5.4 – Summary of final fit results.

Parameter	e+jets	μ+jets
N_S	367 ± 38	400 ± 47
N_B	769 ± 42	1538 ± 58
B_{eff}	0.51 ± 0.04	0.51 ± 0.04

5.5.1 Statistical uncertainty

The statistical uncertainty that is quoted is obtained by performing pseudo-experiments. We applied the fit procedure to 10,000 pseudo-datasets, of which the input parameter values are randomly pulled from the probability density functions that describe them. Specifically, each pseudo-experiment represents a possible set of observed data points. The minimization of the likelihood for this pseudo-dataset works identically to the actual fit, including the implicit constraints that are defined. The fit results are collected to estimate the uncertainties on each parameter of interest. This procedure is used rather than the statistical uncertainty that follows from the minimization of the data fit, because it takes into account that are input parameters are statistically limited as well.

Correlations

We investigate the correlations between the fit parameters. Figure 5.7(a) shows the correlation coefficients in the parametrization we chose:

- B_{eff} (b-tagging efficiency per jet)
- $[\epsilon_B]^1_3$ (background b-tagging efficiency per event)
- N_B (total number of background events)
- N_S (total number of signal events)
- $R_{B43} = \frac{[N_B]_4}{[N_B]_3}$ (ratio between 4-jet and 3-jet slice for background)
- $R_{S43} = \frac{[N_S]_4}{[N_S]_3}$ (ratio between 4-jet and 3-jet slice for signal)

First, it should be noted that the number of signal and background events are highly anti-correlated (-0.75). This is expected, since the total number of events is almost fixed,

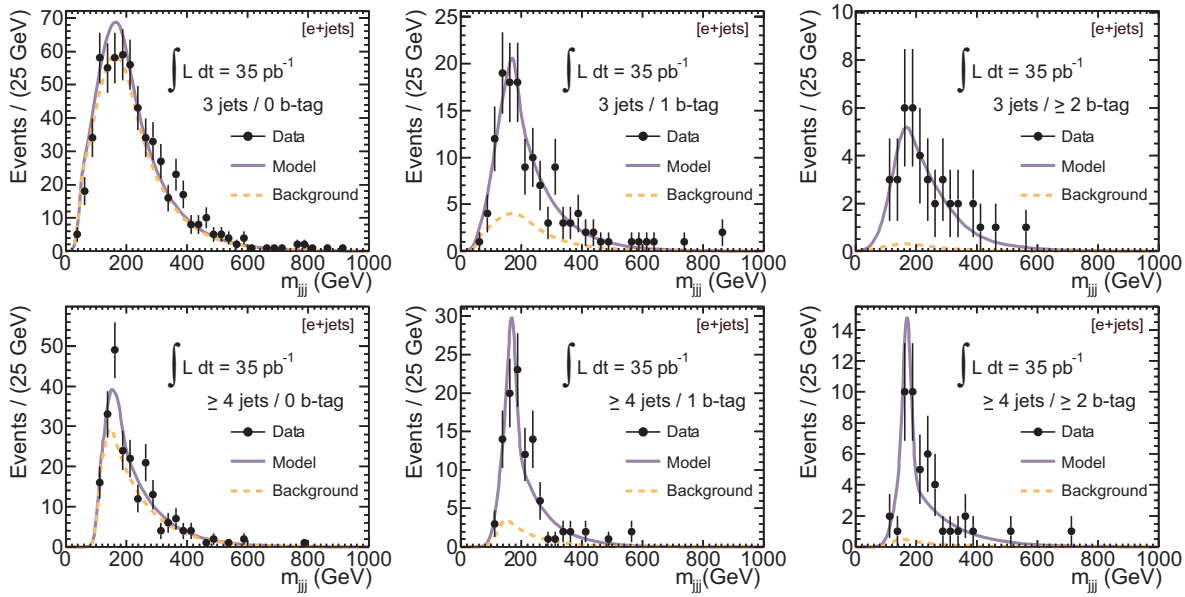

(a)

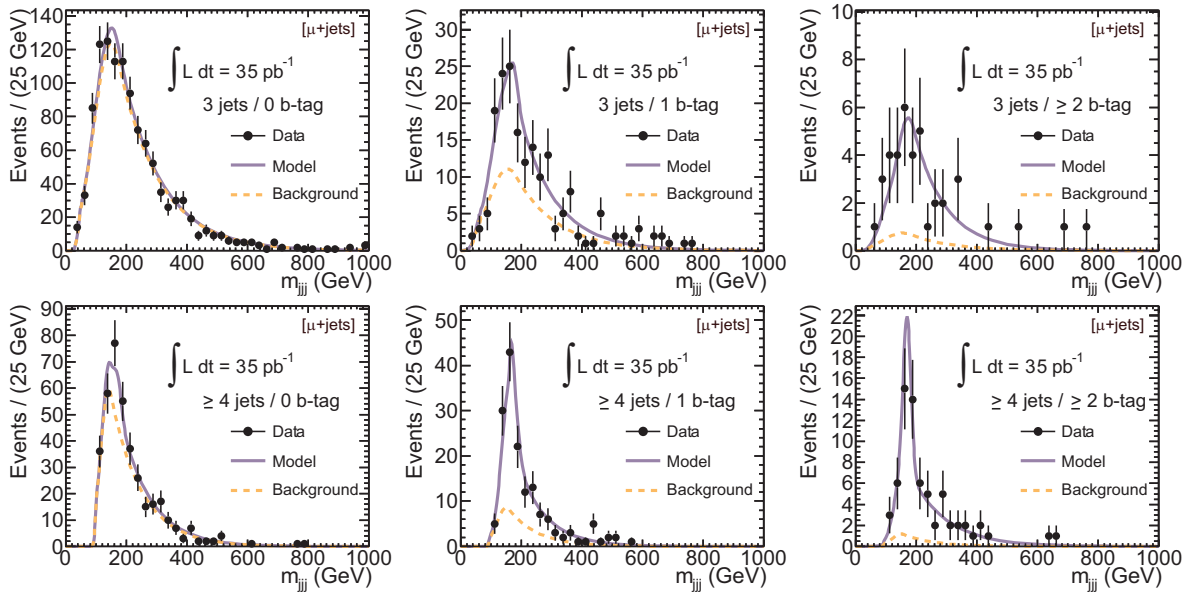

(b)

Figure 5.6 – Fit results in the electron channel (a) and muon channel (b). For each channel the six subsets of the simultaneous fit are shown.

except for the variation allowed by the Poisson extension in the fit. But, B_{eff} and $[\epsilon_B]_3^1$ have a large anti-correlation coefficient with N_S as well. If during the minimization of the fit the number of signal events is pulled towards a higher value, it affects the b-tagging efficiency directly. In other words, if too much signal is present, it has to indicate a lack of b-tagged jets. Likewise, if N_S increases (hence, N_B decreases), the amount of background events in the 3-jet/1-tag slice is reduced. While the direction of such correlations are expected, the magnitude depends strongly on the parametrization that we chose.

In Figure 5.7(b), the correlation (μ-channel) between the b-tag efficiency and the number of signal events (N_S) is shown. The point (black star) at N_S=400, B_{eff}=0.51, corresponds to the final fit result. The squares represent the results of the pseudo-experiment fits. The ellipses indicate the estimated 1σ and 2σ statistical uncertainties. When the fit is applied to simulation (red dot) 433 signal events are measured, with a b-tagging efficiency of 0.53. The simulation is consistent with the 1σ region defined by the pseudo-experiments based on data.

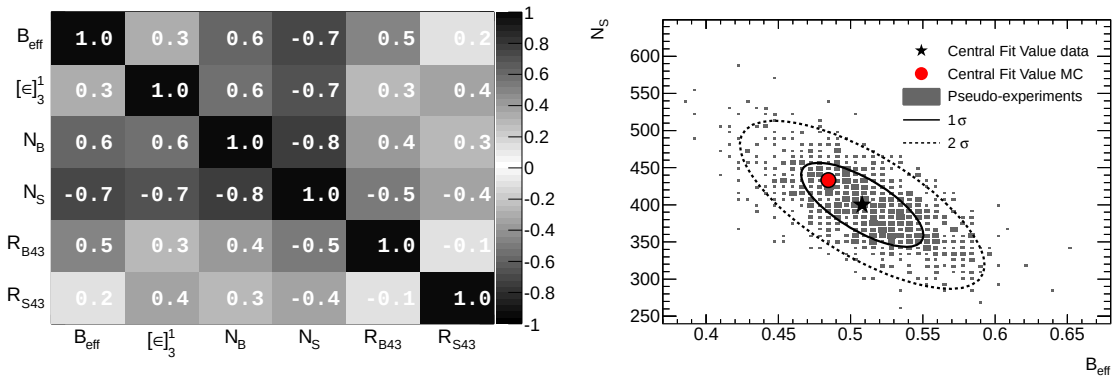

(a) (b)

Figure 5.7 – Correlations in the muon channel. (a) Full correlation matrix. (b) Number of signal events N_S vs. B_{eff}.

5.6 Systematic uncertainties

In this section we describe the treatment and propagation of the uncertainties connected to the cross section values obtained with the simultaneous likelihood fit. An extended view of the final results in terms of the statistical and systematic uncertainties is displayed in Table 5.5.

The effect of each source of systematic uncertainty on the analysis results is determined by varying every parameter within its assessed uncertainty. The parameters that are input to the fit are recalculated considering the deviation and subsequently the fit is reapplied. The impact of a certain nuisance parameter may for instance affect both the estimate of the scale factor $f_{2\to3}$, and the shapes of the distributions. We describe the specific features off systematic uncertainties below.

Table 5.5 – Summary of individual systematic uncertainties contribution to the cross section determination for the fit. All numbers are relative errors expressed as a percentage.

	ΔN(e)/N [%]	**ΔN(μ)/N [%]**	**Combined [%]**
Object selection			
Lepton reco, ID, trigger, scale, smear	± 4.2	± 1.2	± 2.4
Jet energy scale	+2.6/-0.1	+4.5/-0.0	+3.8/-0.0
Jet energy resolution	± 2.4	± 1.0	± 1.6
Jet reconstruction efficiency	± 3.3	± 2.6	± 2.9
b-tagging	+0.4/-1.2	+1.7/-1.2	+1.2/-1.2
Background rate and shape			
Heavy flavor	+5.5/-5.9	+6.3/-5.2	+6.0/-5.5
Shape templates	± 5	± 4	± 4.4
W+jets	+1.8/-1.8	+1.9/-1.9	+1.8/-1.8
Multijet normalization	+5.1/-1.8	+0.5/-0.7	+2.3/-1.1
Signal simulation			
ISR/FSR	+4.2/-4.4	+5.1/-4.4	+4.7/-4.4
PDF	± 1.7	± 1.7	± 1.7
Parton shower	± 0.2	± 0.6	± 0.4
NLO generator	± 2.0	± 1.5	± 1.7
Pile-up	± 0.5	± 0.5	± 0.5
Total			
Sum systematics	+12.3/-11.3	+11.1/-9.1	+11.1/-9.9
Statistical error	±10.5	±11.7	±7.9
Total uncertainty	+17.1/-16.4	+14.7/-13.2	+13.5/12.5

Lepton identification and resolution

The difference between the performance of lepton identification in simulation and data is corrected for with scale factors. The scale factors that incorporate the trigger and reconstruction efficiency difference are supplied by the performance groups in ATLAS using studies of Z boson decays and include statistical and systematic uncertainties. We assume that the quadratic sum of these two in both positive and negative direction models the systematic uncertainty with respect to our final result.

The energy and momentum resolution of the leptons is accounted for as well, by smearing

the simulation such that the distributions match the data. This is done effectively by convolution with a Gaussian probability density function.

Jet energy scale and resolution

The uncertainty on the energy scale of jets is studied in both simulation and data [84]. In data single response studies are performed, comparing the momentum of isolated tracks to the energy deposited in the calorimeter [85]. The simulation studies compare calorimeter jet energies to 'truth jet' energies, the energy of the jet formed directly by a generated particle, skipping the simulation of the detector response. A grid in η-p_T space is defined based on the outcome, with maximal upward and downward shifts for each cell region in this surface. This grid is applied to the nominal values of jet energies to estimate the effect of these variations on the final results. Effects coming from multiple collisions per bunch crossing (pile-up) and of jets in a high jet multiplicity environment (close-by jets) are accounted for as well.

The resolution of the energy and efficiency of finding jets are also estimated from a combination of data and simulation. The resolution in data is larger than in simulation and to resemble this behavior the energy of jets is convoluted with a Gaussian function in the nominal simulation samples. The difference between the results when using the nominal and the non-smeared sample are taken as the 1σ uncertainty. We assess the reconstruction efficiency by discarding a small fraction of jets according to the measured efficiency. This results in a variation as well. Both the jet energy resolution and the reconstruction efficiency generate symmetric uncertainties.

Initial and final state radiation

The uncertainty on initial and final state radiation (ISR/FSR), in the form of extra jets in the detector is estimated by varying parameters in leading-order simulation samples. The effect of more jets primarily influences the selection efficiency and population of the different jet multiplicity categories in the method. On top of that it bears a reduction of the ability to find the right permutations in a top quark reconstruction algorithm. This was studied for a different analysis in more detail in Section 3.5. For the current analysis we used a leading-order $t\bar{t}$ sample where ISR and FSR where increased simultaneously to maximize the effect on the top quark mass. Similarly one sample that minimizes the top quark mass is used. The generator settings are such that the probability of splitting off extra partons is larger or smaller respectively, within reasonable ranges. The final fit result of these two variations is compared with a nominal leading-order sample, instead of the default NLO signal samples to maintain a fair comparison. The relative differences are quoted as the 1σ uncertainty.

Parton density functions

The parametrization of the parton density functions (PDFs) affects the cross section measurement directly. The PDFs describe the probability density of the two partons of the

colliding protons as a function of the longitudinal momentum fractions (x_1,x_2) at energy scale Q^2. PDFs enter the equation of top quark pair production through convolution with the partonic cross section. The full equation is given in Eq. 1.1. The nominal description of PDFs that we use is CTEQ6.6 [86]. Alternatively, MWST2008nlo68cl [33] and NNPDF20 [87] are tested. The estimate of the total uncertainty with respect to the cross section due to PDFs takes input from two distinct parts: the uncertainty within a PDF and the deviations between the different PDFs. The method uses reweighting of events, rather than regeneration. Simulation samples are reweighted according to the ratio of the probabilities of the PDF that is subject to testing (f_{PDF}) and the original PDF (f_{PDF_0}):

$$W = \frac{f_{PDF}(x_1, f_1, Q)}{f_{PDF_0}(x_1, f_1, Q)} \cdot \frac{f_{PDF}(x_2, f_2, Q)}{f_{PDF_0}(x_2, f_2, Q)},$$

where x_1 and x_2 are the momentum fractions of the partons with respective flavors f_1 and f_2. For each PDF an error set is defined, yielding a 1σ variation of one parameter. The CTEQ PDF error set consist of 44 up and down variations originating from 22 parameters. A total error within the PDF is then calculated using

$$\Delta\epsilon = \frac{1}{2}\sqrt{\Sigma_{i=0}(\epsilon_i^+ - \epsilon_i^-)^2},$$

where i is a number corresponding to the varied parameter and $\epsilon_i^{+(-)}$ is the uncertainty on the cross section for the positive (negative) variation. Similar calculations are done for the other two PDF error sets. Finally, a window around the largest upward and downward shift of the cross section of either the different PDF sets or within one PDF is considered. This window therefore includes all reasonably possible values. Half the window size is used as symmetric uncertainty.

NLO generator

The uncertainty on the signal event generator itself (MC@NLO) is evaluated by comparing it to another NLO generator, POWHEG. In this case both generators are interfaced to HERWIG/JIMMY, to keep hadronization and the treatment of the underlying event consistent. The difference in the final result obtained with the two generators is taken to be the symmetric systematic uncertainty. The hadronization and parton showering steps are reproduced in PYTHIA for POWHEG as well, comparing it to HERWIG/JIMMY. Hadronization and parton showering are treated differently for both. Therefore this is a measure for the systematic uncertainty on this step of event simulation. Note that the comparison is not possible with the nominal signal simulation generator MC@NLO the reason being that the interface to PYTHIA is not realized yet.

Pile-up modeling

Pile-up effects are described in Section 4.1.1 for the data set of this analysis. It embodies extra activity in the detector as a result of the occurrence of multiple proton-proton

collisions per bunch crossing. Simulation samples are corrected for this effect, but data-simulation comparisons show residual differences in the tails in terms of the number of reconstructed primary vertices. The simulation of signal and background is therefore reweighted to match the data. This is done by assigning a weight to every event depending on the number of well reconstructed primary vertices that are present. The difference between the final result obtained with the reweighted sample and the original simulation is the symmetric uncertainty quoted in Table 5.5.

Heavy flavor contribution in background

The uncertainty on the quark flavor composition of the $W+$jets background gives rise to a large systematic uncertainty in the measurement of the cross section. Its details have been discussed in the discussion on fit constraint 1 in Section 5.3.1. The same methods described to evaluate the effect on the scale factor were applied to the full analysis to obtain the final results. Variations in the relative contributions of $W+c\bar{c}$, $W+b\bar{b}$ and $W+c$ are produced, in the overall set of events and in specific subsets (jet bins) and the fit is applied to obtain the uncertainty.

Background rate

The amount of background is a fit parameter and does in principle not need to be accounted for. The only way the uncertainty on the rate of background events enters is through R_1 and R_3, which are ratios and therefore only moderately dependent on the overall normalization. Nevertheless, this effect is computed by varying the rates of the individual backgrounds and redoing the calculations of scale factors and perform the fit. The result is the difference between the cross section results obtained with the modified rates and the nominal value. On the simulated backgrounds a 1σ variation on the generator cross section is applied. The multijet contributions (data-driven) have an uncertainty assigned in the procedure of obtaining the rate from data. It is varied accordingly, up an down, to estimate the change in the final outcome. The $W+$jets uncertainty quoted in the table comes from a test where the events are generated with a different generator (Sherpa) and show only small deviations.

Template shapes

The effect of the uncertainty of the shapes of the templates is tested by taking 'flat' templates, i.e., each template is described by a horizontal function. This reduces the fit towards a 'counting experiment' effectively. This is assumed to be the most extreme case.

Calibration of b-tagging

The b-tagging efficiency uncertainty is fitted for in case of signal. In background, however, it plays an important role in combination with the heavy flavor uncertainty. The uncertainty on the calibration is assessed by varying the scale factors used in the procedure of

matching simulation to data, within their uncertainty.

Luminosity

The uncertainty on the measurement of the luminosity was 3.4% at the time the measurement was performed [88].

5.7 Cross section results

The cross section can be expressed as

$$\sigma(t\bar{t}) = \frac{N_S}{\int \mathcal{L}dt \cdot \epsilon},$$

where the efficiency ϵ incorporates the trigger efficiency, acceptance and top quark reconstruction efficiency. We applied the fit to the data distributions in the muon and electron channel separately. The number of signal events in data is N_S is 367 ± 44 (stat) for the electron channel and 400 ± 38 (stat) for the muon channel. This translates to the cross sections listed in Table 5.6. The individual results are quoted per channel, as well as a combined statistical combination.

Table 5.6 – Summary of final cross section estimates.

Channel	Cross section
e + jets	216 ± 23 (stat) $^{+27}_{-24}$ (syst) ± 7 (lumi) pb
μ + jets	161 ± 19 (stat) $^{+18}_{-15}$ (syst) ± 5 (lumi) pb
Combined e/μ + jets	183 ± 14 (stat) $^{+20}_{-18}$ (syst) ± 6 (lumi) pb

The results are in agreement with theoretical expectations at NNLO [35],

$$\sigma_{t\bar{t}} = 158.7^{+12.2}_{-13.5}\ (\text{scale})\ ^{+4.3}_{-4.4}\ (\text{PDF})\ \text{pb}.$$

Figure 5.8 reflects the theoretical prediction for top quark pair production at pp and $p\bar{p}$ colliders in blue and yellow, including the 1σ error band. The best measurements at the Tevatron are included. The combined result of the fit analysis in this chapter is shown in the large plot, and the individual results are compared in the smaller box. The electron fit result is higher than expected, but still within 2σ from the expectation. The muon channel agrees with the theoretical expectations. The combined result is consistent with the predictions as well. The uncertainty of this measurement, however, is not at the level of the theoretical uncertainties yet.

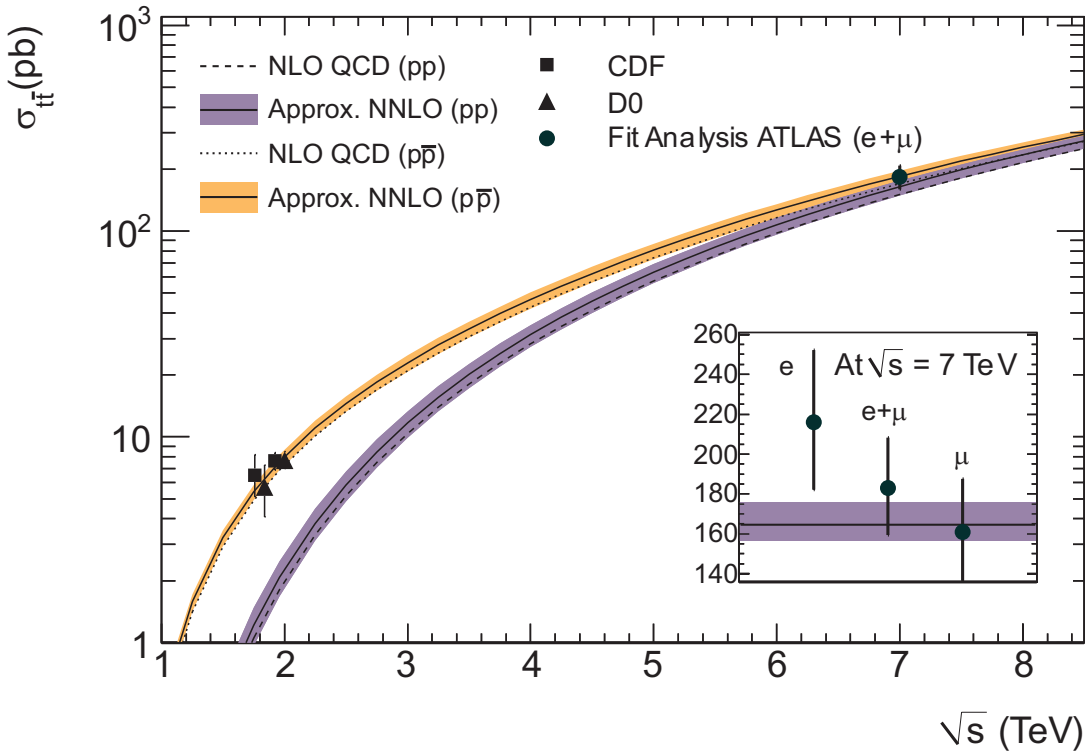

Figure 5.8 – Cross section versus CM-energy $\sqrt{s}$. The cross section results of this chapter are overlaid to the theoretical predictions at (N)NLO. The individual values for the separate channels are shown in the inset.